Journal of Visualization, Vol. 8, No. 4 (2005)295-303

# Flow Characteristics around a Rotating Grooved Circular Cylinder with Grooved of Different Depths

Takayama, S.*[1] and Aoki, K.*[2]

*1 Tokai University, Graduate School of Engineering, Course of Mechanical Engineering, 1117 Kitakaname, Hiratsuka, Kanagawa, 259-1292, Japan.
*2 Tokai University, Department of Mechanical Engineering, School of Engineering, 1117 Kitakaname, Hiratsuka, Kanagawa, 259-1292, Japan.

Received 8 July 2004
Revised 12 July 2005

***Abstract***: The present paper describes the flow characteristics around a rotating grooved circular cylinder with grooves of different depths. The surface structure of a circular cylinder was varied by changing the depths of 32 arc grooves on the surface. The surface pressure on the cylinder is measured for the $Re$ range of from $0.4\times10^5$ to $1.8\times10^5$ and for rotations of from 0 to 4500 rpm. The drag coefficient of a grooved cylinder increases as the spin rate ratio $\alpha$ (= rotational speed of the cylinder surface/uniform velocity) increases for $Re > 1.0\times10^5$. As the groove depth increases, the drag coefficient of a grooved cylinder is independent from the spin rate ratio $\alpha$. The direction of the lift force of a smooth cylinder is opposite to the Magnus force for $Re > 1.0\times10^5$. However, the direction of the lift force of a grooved cylinder is the same as that of the Magnus force for all $Re > 1.0\times10^5$. As the groove depth increases, the increase in the slope of the lift coefficient becomes small. These phenomena are related to the positions of the flow separation points, which are clarified from the pressure distribution and flow visualization by the spark tracing method. In addition, in the present study, the flow around a rotating grooved cylinder is clarified by flow visualization.

***Keywords***: Rotating cylinder, Spark tracing method, Fluid force, Pressure distribution.

## 1. Introduction

The drag and lift of a circular cylinder in a uniform flow have been reported widely in the literature (Schewe, 1983; Roshko, 1961; Osawa and Tezduyar, 1999; Gushchin et al., 2004). In the case of a stationary smooth cylinder, the drag coefficient shows a characteristic change as the Reynolds number changes. In general, the drag coefficient for a smooth cylinder may be classified into three regions, subcritical, critical and supercritical, as the Reynolds number increases. The critical region for a smooth cylinder is at $Re = 3.5\times10^5$. The drag coefficient characteristics for the surface structure of circular cylinders have been clarified by Achenbach (1971); Achenbach and Heinecke (1981). As the roughness of the surface of the circular cylinder increases, the critical point shifts to lower Reynolds numbers and the drag coefficient of a rough cylinder is smaller than that of a smooth cylinder. However, for rough cylinders, as the Reynolds number increases further, the drag coefficient increases. Aoki et al. (2003) reported that for a grooved cylinder (regular roughness), the critical Reynolds number is smaller than that for a circular cylinder without grooves. Swanson (1961) reported the drag and lift characteristics of a rotating smooth cylinder with respect to the spin rate

ratio $a$ and also reported that the lift of a rotating smooth cylinder generates a negative force. In addition, Diaz et al. (1983) reported the existence of Karman vortex shedding by a rotating smooth cylinder at $Re = 9000$. However, the flow characteristics of a circular cylinder with a changing surface structure have not yet been reported. Therefore, in the present study, the flow characteristics of a rotating grooved circular cylinder with grooves of various depths are clarified by means of the pressure distribution and the spark tracing method.

# 2. Experimental Apparatus

## *2.1 Pressure Measurement*

The experiments were conducted in a blow-down wind tunnel having a width of 180 mm and height of 380 mm. The air velocity was varied from 7 to 35 m/s ($Re = 0.4\times10^5 \sim 1.8\times10^5$). The turbulence level for this range was approximately 0.6%. The cylinder was rotated at 0 ~ 4500 rpm. Figure 1 shows the rotating test cylinder. The diameter of the test cylinder d is 80 mm. There are 32 arc grooves on the surface of the cylinder. The pressure holes on the cylinder surface are located at two positions, outside and inside the grooves, respectively. The diameter of the pressure holes is 0.8 mm. Two pressure transducers installed inside the cylinder were used to measure the surface pressures of the rotating cylinder. Electrical signals from the transducers were converted from a rotating condition to a static condition by means of a slip ring. The width of each groove is 6.76 mm, and the depths of the grooves are varied to three depths, as listed in Table 1. The length in the span direction of the test cylinder is 172 mm, and disks of 110 mm in diameter were placed at the ends of the cylinder in order to prevent secondary flow.

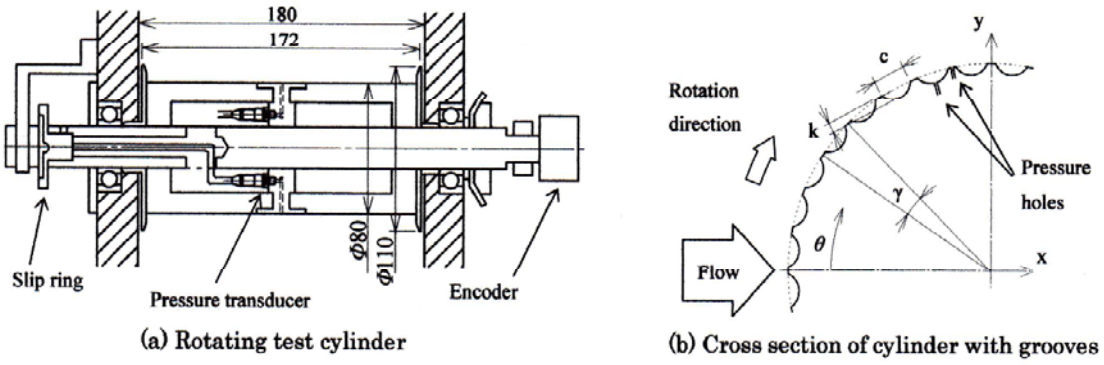


(a) Rotating test cylinder (b) Cross section of cylinder with grooves

Fig. 1. Experimental apparatus for measuring of surface pressure.

Table 1. Specification of cylinder.

| Type | A | B | C |
|---|---|---|---|
| k (mm) | 0.30 | 0.58 | 0.94 |
| d (mm) | 80 | | |
| c (mm) | 6.76 | | |
| γ (deg) | 11.25 | | |
| k/d | $3.75\times10^{-3}$ | $7.25\times10^{-3}$ | $11.75\times10^{-3}$ |

### *2.2 Flow Visualization by Spark Tracing Method*

Figure 2 shows the experimental apparatus used for the spark tracing method. The pulse generator can generate pulse waves of high voltage electricity. The electricity is stored in a pulse drive unit

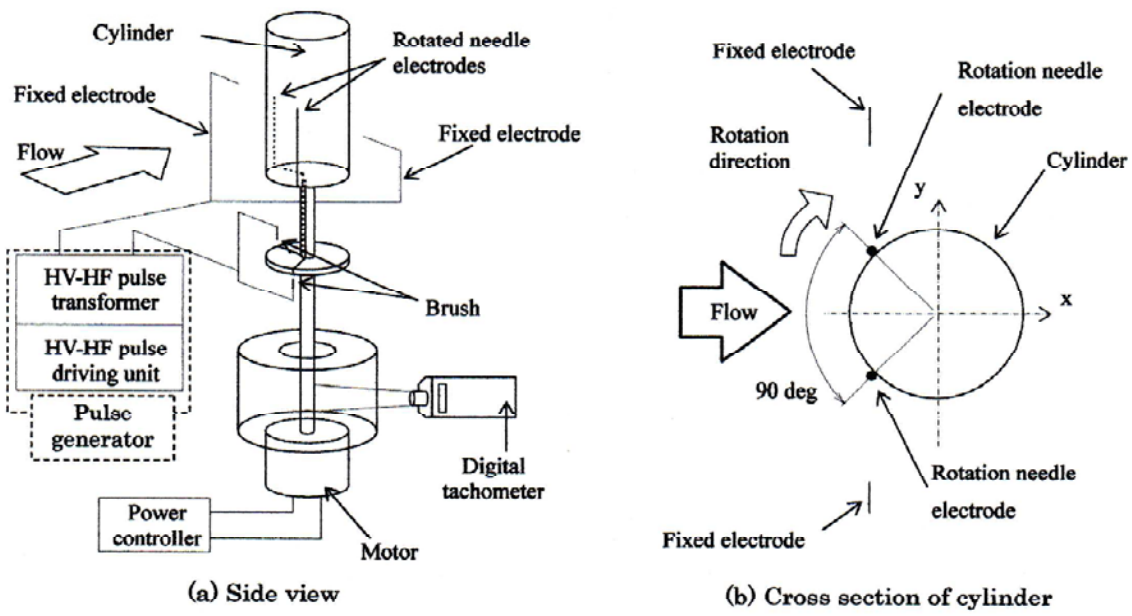


Fig. 2. Experimental apparatus for spark tracing method.

and then passed through a pulse transformer and a fixed electrode. Brushes contact the rotating needle electrodes and the fixed electrode, and the rotating needle electrodes discharge sparks. The electrode material is tungsten, and the diameter of the electrode is 0.1 mm. The first electric spark from the pulse wave arcs to another electrode over the shortest distance, producing ionized air after the first electric spark. This ionized air moves together with the uniform flow. The second electric spark from the pulse wave passes through this ionized air because the electric resistance of the ionized air is low, and the second electric spark again produces ionized air. The ionized air from the second electric spark moves together with the uniform flow, and the third electric spark moves again through the ionized air from the second electric spark. The flow pattern around the rotating cylinder can be visualized by repeating this process.

## 3. Results and Discussion

### *3.1 Drag and Lift Coefficients without Rotation*

Figure 3 shows the drag coefficient $C_D$ and lift coefficient $C_L$ of the test cylinder without rotation. The drag and lift coefficients are calculated by integrating the pressure distribution. For the Reynolds number range investigated herein, the drag coefficient of a smooth cylinder is constant at approximately 1.25. For the Type A cylinder, the drag coefficient decreases as the Reynolds number increases, and the increase is gradual for $Re > 0.9\times10^5$. For $0.6\times10^5 < Re \leq 0.9\times10^5$, the drag coefficient decreases, indicating the critical region, and for $Re > 0.9\times10^5$, the drag coefficient indicates the supercritical region. The critical region of the grooved cylinder shifts to the low Reynolds number side as the groove depth increases, and the Type C cylinder, which has the deepest grooves, shows only a supercritical region.

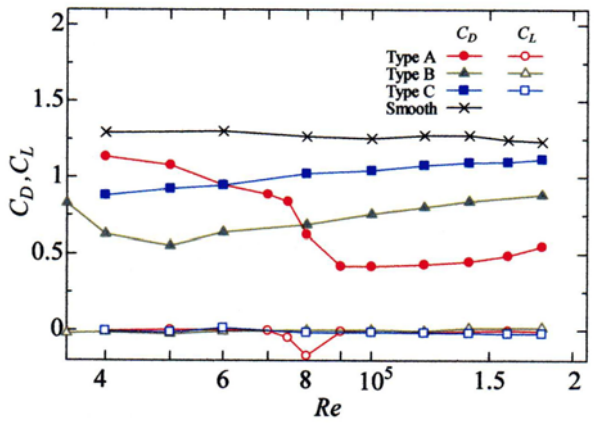


Fig. 3. Drag and lift coefficients of stationary condition.

### *3.2 Drag and Lift Coefficients of the Rotating Condition*

Figures 4 and 5 show the drag coefficient $C_D$ and lift coefficient $C_L$ of the rotating smooth cylinder and the rotating grooved cylinder in relation to the spin rate ratio $\alpha$. The drag and lift coefficients are calculated from the pressure distribution.

In the case of a smooth cylinder, the drag coefficient decreases when the spin rate ratio $\alpha$ is 0.6 at $Re = 0.4\times10^5$. This area of decreasing drag coefficient moves toward lower spin rate ratio $\alpha$ as the Reynolds number increases. The lift coefficient increases after decreasing and becomes negative at $Re \geq 1.0\times10^5$. Moreover, the lift coefficient approaches 1.0 for all Reynolds numbers cases. Thus, the drag and lift coefficients of the rotating smooth cylinder change suddenly at a certain spin rate ratio,

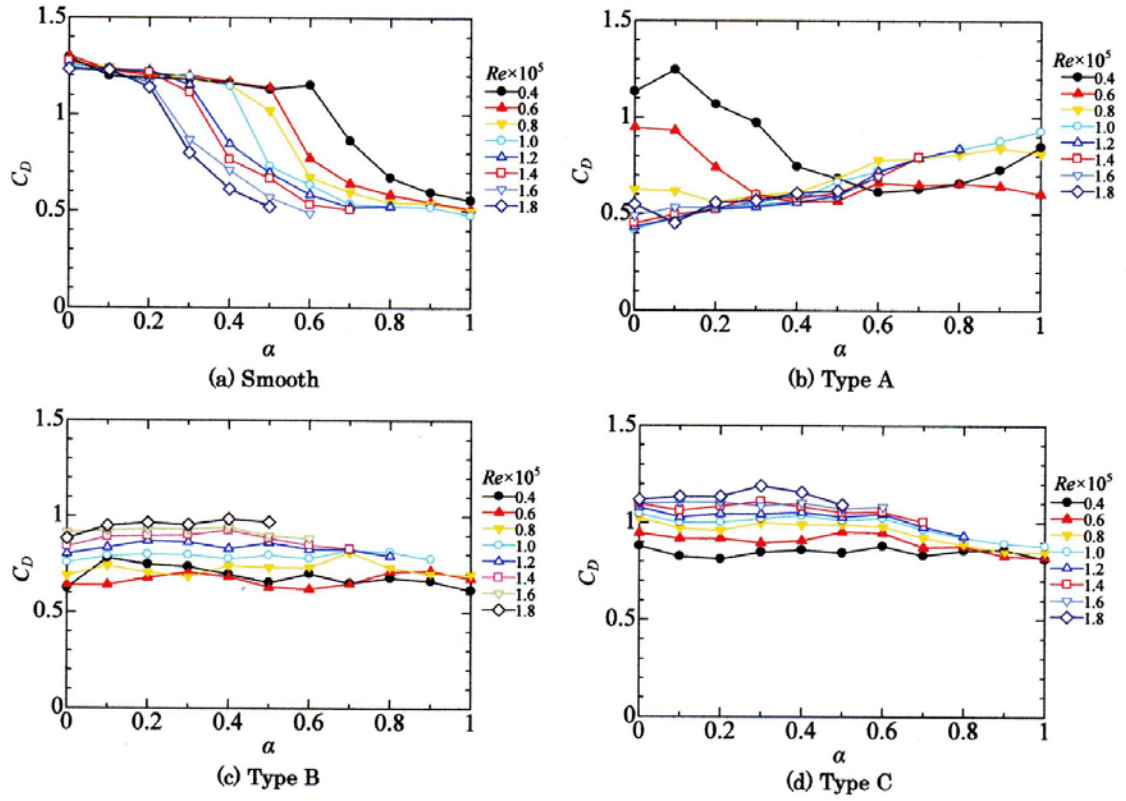


Fig. 4. Drag coefficient of rotating cylinder with grooves.

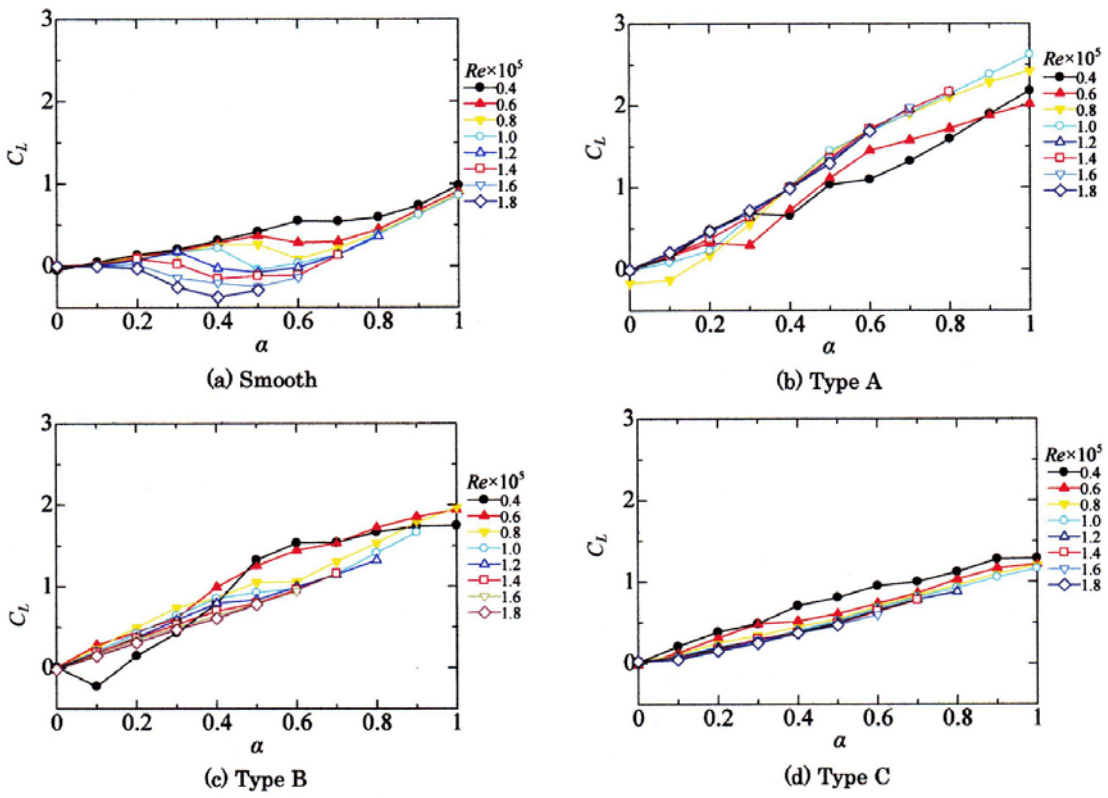


Fig. 5. Lift coefficient of rotating cylinder with grooves.

because the boundary layer of the deceleration side changes from laminar flow to turbulent flow. For the Type A cylinder, the drag coefficient decreases and then increases as $\alpha$ increases at a Reynolds number of $Re = 0.4\times10^5$. However, the drag coefficient increases almost monotonically at $Re \geq 1.0\times10^5$, and the lift coefficient increases monotonically with $\alpha$ at $Re \geq 1.0\times10^5$. At $Re < 0.8\times10^5$, the lift coefficient increases after it decreases once as $\alpha$ increases. For the Type B cylinder, the lift coefficient increases after decreasing at a Reynolds number of $Re = 0.4\times10^5$. For $Re > 0.4\times10^5$, the lift coefficient increases monotonically as $\alpha$ increases. For the Type C cylinder, the lift coefficient increases monotonically as $\alpha$ increases for all Reynolds numbers. As the groove depth increases, the increase in the slope of the lift coefficient becomes small. The drag coefficients of the Type B and Type C cylinders are not affected by large increases in $\alpha$, and the drag coefficient of the Type C cylinder is considered to be larger than that of the Type B cylinder because the wake area of the Type C cylinder is larger as discussed later. Thus, the lift and drag coefficient characteristics under the rotating condition depend on the lift and drag characteristics without rotation.

### *3.3 Pressure Distribution*

Figure 6 shows the pressure distributions for the rotating smooth cylinder and the rotating grooved cylinder for spin rate ratios $\alpha$ ranging from 0 to 0.9 at $Re = 1.0\times10^5$. As $\alpha$ increases, the pressure distribution shifts downward in this figure. The pressure coefficient $C_P$ is expressed as follows:

$$C_P = \frac{p - p_s}{\rho u^2 / 2} \tag{1}$$

where $p$ is the pressure on the cylinder surface, $p_s$ is the static pressure, $\rho$ is the density of air and $u$ is the uniform velocity.

In this figure, the acceleration side is from 0 to 180 deg, and the deceleration side is from 180 to

360 deg. The measured pressure is calibrated based on authors (Takayama and Aoki, 2003). In the pressure distribution of the rotating smooth cylinder, the acceleration side and deceleration side become asymmetrical as $a$ increases. At $a < 0.5$, the negative peak of $C_p$ of the acceleration side is clear, but that on the deceleration side is not, and at $a = 0.4$, the drag coefficient decreases suddenly and the lift coefficient becomes negative as shown in Figs. 4(a) and (5). Then, the separation point is determined as the point at which the pressure distribution becomes constant. For the case in which the pressure distribution vibrates near the separation point, the separation point is determined as the distribution peak. The separation point of the acceleration side moves downstream as $a$ increases, and that of the deceleration side shifts downstream suddenly at $a = 0.4$~$0.5$. For a smooth cylinder without rotation $Re = 1.0\times10^5$ is the subcritical region, and the flow on the cylinder surface is laminar. As $a$ increases, the fluid on the surface of the acceleration side trails downstream, because the rotation direction of the acceleration side is the same as the direction of the flow, and the separation point also moves downstream. However, the rotation direction of the deceleration side and the direction of the uniform flow are opposite to each other and the relative speed increases as $a$ increases. Therefore, the boundary layer of the deceleration side changes to turbulent flow, and the separation point of the deceleration side shifts downstream at $a = 0.4$~$0.5$. For a grooved cylinder, in Fig. 6(b), (c), and (d) the solid line shows the pressure coefficient $C_P$ outside the grooves, and the

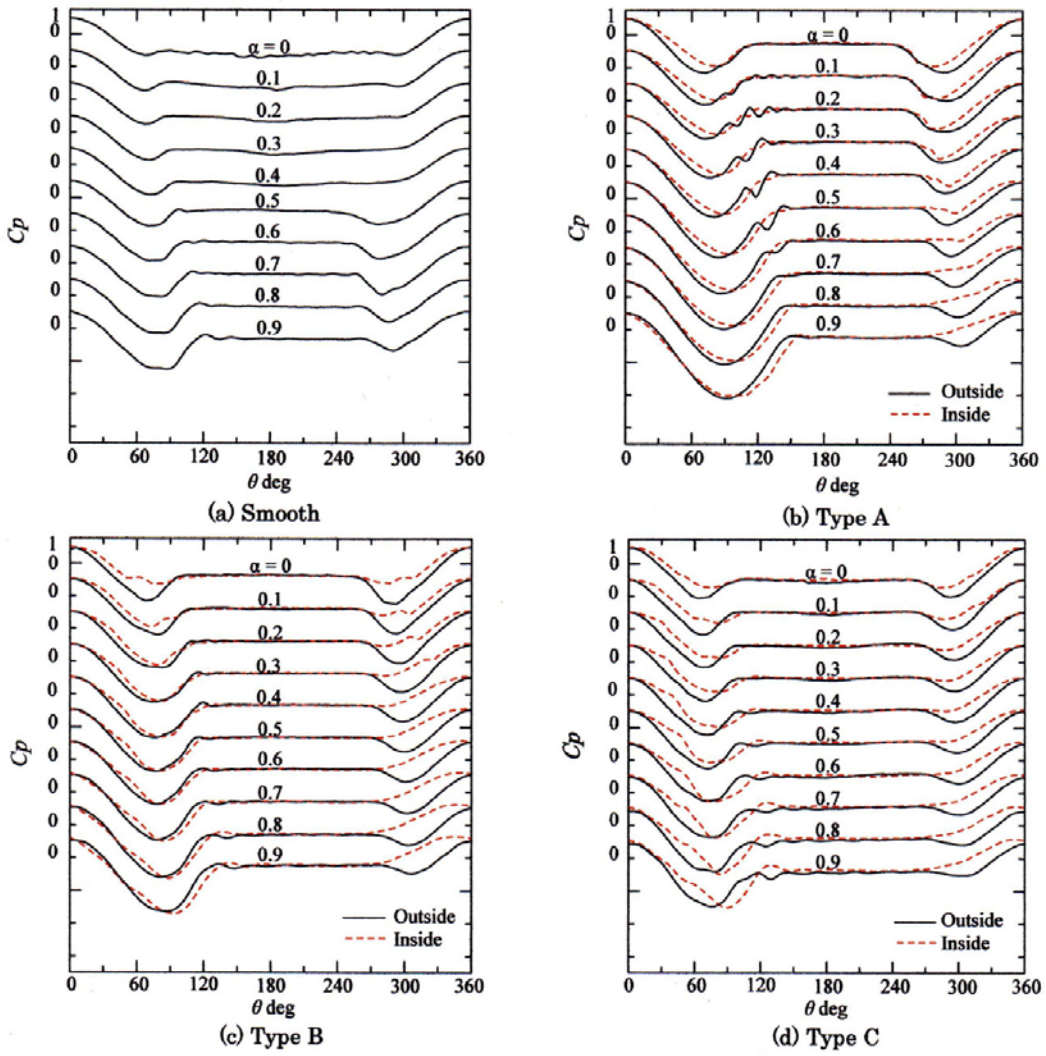


Fig. 6. Pressure distribution ($Re = 1.0\times10^5$).

broken line shows that inside the grooves. As $a$ increases, the separation point of the acceleration side moves downstream, and the separation point of the deceleration side gradually moves upstream. The boundary layer flow of the grooved cylinders is already turbulent flow $a = 0$, and the separation point of the deceleration side does not move downstream as $a$ increases. As the grooves depth increases, the separation point on the acceleration side moves upstream and the wake area becomes large. Moreover, as the groove depth increases, the minimum $C_P$ of the acceleration side increases.

### *3.4 Flow Visualization*

Figures 7 and 8 show the visualization results obtained by the spark tracing method at $Re = 1.0\times10^5$. The visualization results show the flow pattern around a rotating grooved cylinder and the wake flow, and indicate that the separation point changes as $a$ increases. When the smooth cylinder is rotated, the separation points move in the rotation direction. However, the separation point of the deceleration side shifts downstream at $a = 0.5$. Therefore, the wake area is reduced and the drag coefficient becomes small. The separation points of the acceleration side and the deceleration side become symmetric, and the lift coefficient becomes small. In the case of the Type A cylinder, the separation points always move in the rotation direction as $a$ increases. The wake area of the grooved cylinder is smaller than that of the smooth cylinder, and so the drag coefficient of the grooved cylinder becomes small. At $a = 0.4$, the wake area of the grooved cylinder moves further in the rotation direction compared to the smooth cylinder. Therefore, the lift coefficient of the grooved cylinder becomes greater than that of the smooth cylinder. As the groove depth increases, the size of the wake area becomes larger. As $a$ increases, the size of the wake area becomes small, and thus the drag coefficient changes smaller. The separation point moves in the rotation direction as $a$ increases, and the movement of the separation point decreases as the grooves become deeper.

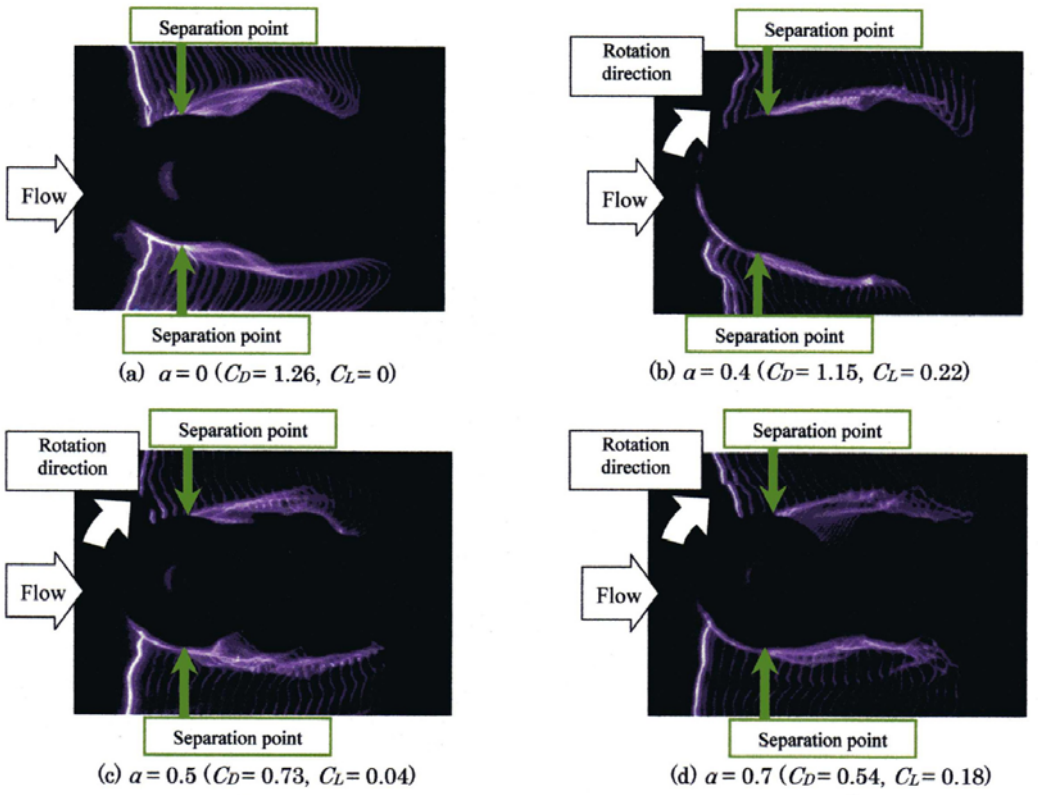


Fig. 7. Flow visualization of smooth cylinder ($Re = 1.0\times10^5$).

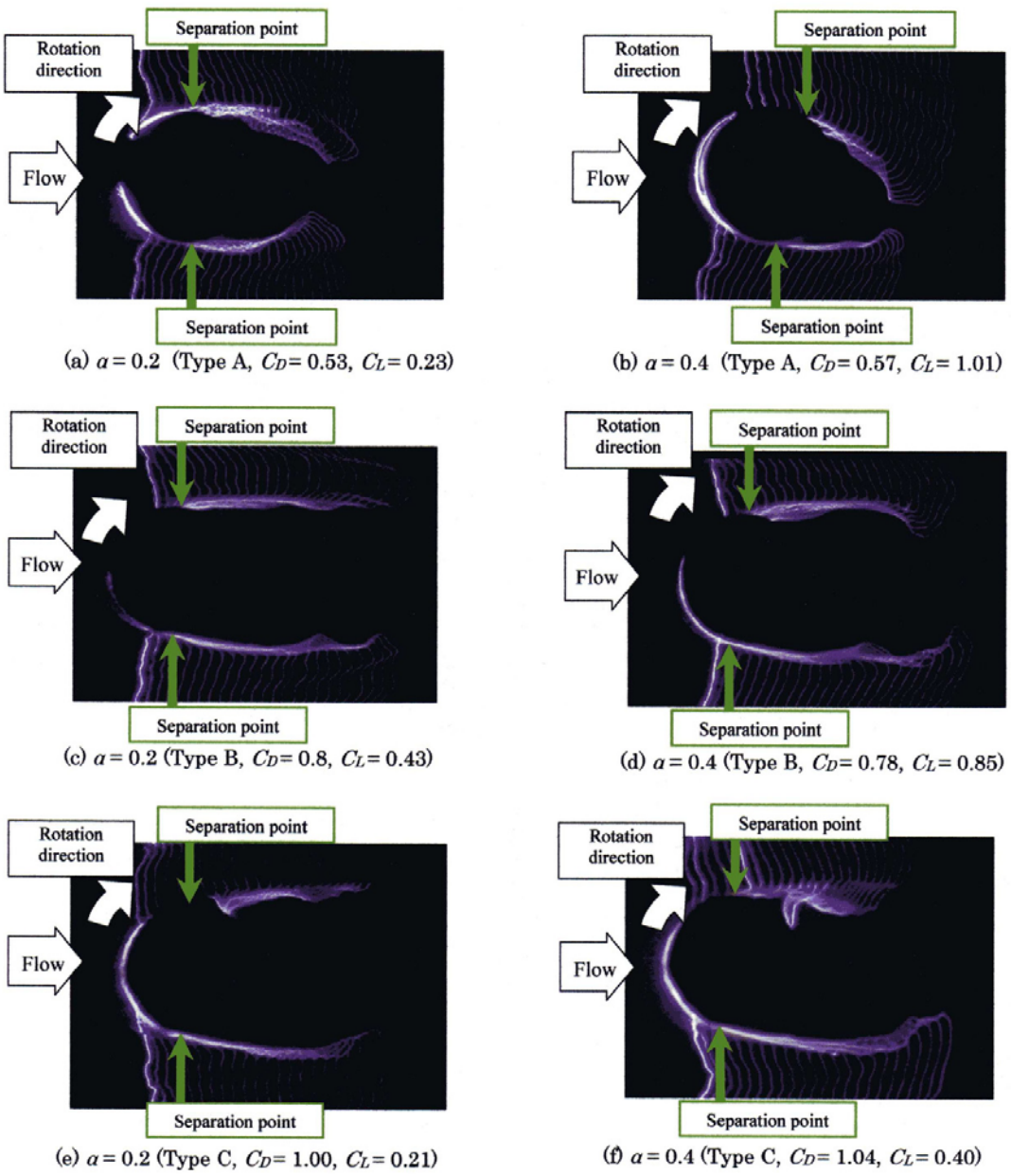


Fig. 8. Flow visualization of cylinder with grooves ($Re$ = $1.0\times10^5$).

Accordingly, the increase in the slope of the lift coefficient becomes smaller as the grooves become deeper.

## 4. Conclusions

The experimental results for a rotating a cylinder with arc grooves revealed the following:

1. The drag coefficient of the smooth cylinder decreases at a certain spin rate ratio. The drag coefficient of the grooved cylinder shows area of decreasing drag coefficient only for Reynolds numbers of the subcritical and critical regions without rotation.
2. The drag coefficient of a grooved cylinder with grooves does not depend on the spin rate ratio as

the grooves become deeper.

3. The lift coefficient of a smooth cylinder decreases at a certain spin rate ratio. At $Re \geq 1.0\times10^5$, the lift coefficient of a smooth cylinder becomes negative. The lift coefficient of a grooved cylinder decreases at a certain spin rate ratio for Reynolds numbers in the subcritical and critical regions without spin.
4. The lift coefficient of a grooved cylinder increases monotonically for Reynolds numbers in the supercritical region without spin, and the increase in the slope of the lift coefficient becomes smaller as the grooves become deeper.
5. In the case of a smooth cylinder, the separation point of the deceleration side moves downstream at $Re = 1.0\times10^5$ and $\alpha = 0.5$, whereas, in the case of a grooved cylinder, the separation point moves only in the rotation direction as $\alpha$ increases at $Re = 1.0\times10^5$.

## *References*


Achenbach, E., Influence of surface roughness on the cross-flow around a circular cylinder, J. Fluid Mech., 46-2 (1971), 321-335.

Achenbach, E. and Heinecke, E., On vortex shedding from smooth and rough cylinders in the range of Reynolds number $6\times10^3$ to $5\times10^6$, J. Fluid Mech., 109 (1981), 239-251.

Aoki, K., Shimada, T. and Takayama, S., Flow Characteristics around Circular Cylinder with Arc Grooves, Proc 7th Asian Symposium on Visualization, Singapore, (2003).

Diaz, F., Gavaldá, J., Kawall, J. G., Keffer, J. F. and Giralt, F., Vortex shedding from a spinning cylinder, Phys. Fluids, 26-12 (1983), 3454-3460.

Gushchin, V. A., Kostomarov, A. V. and Matyushin, P. V., 3D Visualization of the Separated Fluid Flows, Journal of Visualization, 7-2 (2004), 143-150.

Osawa, Y. and Tezduyar, T., 3D Simulation and Visualization of Unsteady Wake Flow behind a Cylinder, Journal of Visualization, 2-2 (1999), 127-134.

Roshko, A., Experiments on the flow past a circular cylinder at very high Reynolds number, J Fluid Mech., 10 (1961), 345-356.

Schewe, G., On the force fluctuations acting on a circular cylinder in crossflow from subcritical up to transcritical Reynolds numbers, J. Fluid Mech., 133 (1983), 265-285.

Swanson, W. M., The Magnus Effect: A Summary of Investigations to Date, Transactions of ASME, 83 (1961), 461-470.

Takayama, S., and Aoki, K., Pressure Response Characteristics of a Measurement System for a Rotating Cylinder, Proc the school of engineering of Tokai University. 43-1 (2003), 73-77 (in Japanese).


## *Author Profile*

Shinichi Takayama: He received his M. Sc. (Eng.) in Mechanical Engineering in 2002 from Tokai University. He also received his Ph.D. in Mechanical Engineering in 2005 from Tokai University.

Katsumi Aoki: He received his M. Sc. (Eng.) degree in Mechanical Engineering in 1976 from Tokai University and his Ph. D. in Mechanical Engineering in 1986 from the same University. After obtaining M. Sc. he worked as a research assistant, a lecturer, and an associate professor at Tokai University before taking up his current position as a professor of Tokai University. His current research interest covers flow around a rotating circular cylinder with and without grooves, flow around a rotating sphere, possibility of drag reduction using triangle-type cavity and flow visualization by spark tracing method of complicated flow like in centrifugal blower.